GFZ

Helmholtz-Zentrum
POTSDAM

Originally published as:

Colour remote sensing of the impact of artificial light at night (I): The potential of the International Space Station and other DSLR-based platforms

Alejandro Sánchez de Miguel[a,b,c,d,*], Christopher C.M. Kyba[e,f], Martin Aubé[c], Jaime Zamorano[b], Nicolas Cardiel[b], Carlos Tapia[b], Jon Bennie[a], Kevin J. Gaston[a,g]

[a] *Environment and Sustainability Institute, University of Exeter, Penryn, Cornwall TR10 9FE, UK*
[b] *Depto. Física de la Tierra y Astrofísica, Instituto de Física de Partículas y del COSMOS (IPARCOS), Universidad Complutense, Madrid, Spain*
[c] *Physics dept., CEGEP de Sherbrooke, Sherbrooke, J1E 4K1, Canada*
[d] *Instituto de Astrofísica de Andalucía, Glorieta de la Astronomía, s/n, C.P.18008 Granada, Spain*
[e] *Remote Sensing, German Center for Geosciences GFZ, Telegrafenberg, 14473 Potsdam, Germany*
[f] *Ecohydrology, Leibniz Institute of Freshwater Ecology and Inland Fisheries, Muggelseedamm 310, Berlin 12587, Germany*
[g] *Wissenschaftskolleg zu Berlin, Institute for Advanced Study, Wallotstrasse 19, 14193 Berlin, Germany*

ARTICLE INFO

ABSTRACT

Sensors on remote sensing satellites have provided useful tools for evaluation of the environmental impacts of nighttime artificial light pollution. However, due to their panchromatic nature, the data available from these sensors (VIIRS/DNB and DMSP/OLS) has a limited capacity accurately to assess this impact. Moreover, in some cases, recorded variations can be misleading. Until new satellite platforms and sensors are available, only nighttime images taken with DSLR cameras from the International Space Station (ISS), airplanes, balloons or other such platforms can provide the required information. Here we describe a theoretical approach using colour-colour diagrams to analyse images taken by astronauts on the ISS to estimate spatial and temporal variation in the spectrum of artificial lighting emissions. We then evaluate how this information can be used to determine effects on some key environmental indices: photopic vision, the Melatonin Suppression Index, the Star Light Index, the Induced Photosynthesis Index, production of NO_2-NO radicals, energy efficiency and CO_2 emissions, and Correlated Colour Temperature. Finally, we use the city of Milan as a worked example of the approach.

1. Introduction

Artificial nighttime lighting, from streetlights and other sources, has diverse and problematic environmental impacts. These include effects on the physiology, behaviour and phenology of organisms (Dominoni et al., 2013; Dwyer et al., 2013; Altermatt and Ebert, 2016; Bennie et al., 2016), the abundance and distribution of species (Gaston and Bennie, 2014), their ecological interactions (Davies et al., 2013), the composition of communities (Davies et al., 2017), and ecosystem processes and services (Hölker et al., 2015). The severity of all of these impacts depends critically on the spectrum of the lighting (Gaston et al., 2014; Schroer and Hölker, 2016), and thus to map the associated patterns of risk and how these are changing it is essential to have spatial and time series data on the spectral composition of light pollution.

Unfortunately, obtaining information about the spectra of the emissions of outdoor artificial light sources on large spatial scales has

been challenging. The main sources of remote-sensed nighttime lighting data have been colourblind (i.e. single broad band; Elvidge et al., 1999; Liao et al., 2013; Levin et al., 2014; Kyba et al., 2014), and hyperspectral and multispectral data have only been available for a few specific locations photographed as a part of research campaigns (Birmingham - Hale et al., 2013, Berlin - Kuechly et al., 2012; Sánchez de Miguel, 2015, Madrid - Sánchez de Miguel, 2015, Catalonia - Tardà et al., 2011, Las Vegas - Metcalf, 2012, Upper Austria - Ruhtz et al., 2015). There are some new cubesat missions currently exploring the possibilities of nocturnal remote sensing (Walczak et al., 2017; Zheng et al., 2018), in the future there is likely to be access to hyperspectral data from satellites like TEMPO (Carr et al., 2017) and potentially also from Sentinel 4 or 5b, and there have been calls for a dedicated "nightsat" satellite (Elvidge et al., 2007, 2010). But multispectral data are already urgently required. This is particularly the case because rapid changes in the spectra of artificial nighttime lighting are currently

---

taking place (Kyba et al., 2014, 2017). For several decades outdoor lighting has mainly made use of High Pressure Sodium (HPS), Low Pressure Sodium (LPS), metal halide (MH) and fluorescent lamps. However, there are now widespread shifts to ' white' light-emitting diode (LED) lamps, that are projected soon to become the dominant source, and emissions from which have repeatedly been found to have more severe environmental impacts (Davies et al., 2017, 2014).

An alternative, and thus likely vitally important, source of remotely sensed spatial and temporal data on the spectrum of artificial nighttime lighting is photographs taken by astronauts on the International Space Station (ISS). Nocturnal images are available from 2003 to the present, although their temporal and spatial distributions are variable. Between 2003 and 2010, a total of 35,995 nighttime images were taken, with a further 423,520 between 2011 and November 2014. Of these, at least 30,000 images are of cities at night (Sánchez de Miguel et al., 2014; Sánchez de Miguel, 2015). In this paper, we first present a method to classify outdoor lighting types from ISS imagery, using colour-colour diagrams (which can also be used for similar images obtained from remote sensing aerial or ground based platforms). We then determine the relations between the spectral information that can be obtained from the imagery and some key environmental indices (photopic vision, the Melatonin Suppression Index, the Star Light Index, the Induced Photosynthesis Index, production of NO_2-NO radicals, energy efficiency and CO_2 emissions, and Correlated Colour Temperature). Finally, we provide an example of the application of this approach to ISS imagery of the city of Milan.

Throughout, we concentrate on the underlying principles of the approach. For practical application, calibration and instrument effects also need to be considered, and these will be explained in a future paper. We focus here on establishing the principles using Nikon DSLR cameras as the exemplar, because these are the ones used on the ISS. A similar technique can be applied to any other RGB camera. With the primary exception of astronomical CCD cameras and some professional cameras, current digital cameras use a Bayer matrix filter to create the final colour image. The characteristics of these filters can change from one brand to another. One of the advantages of Nikon cameras is that recent models have been very consistent in their spectral response. Thus, whilst we will concentrate on the spectral response of the Nikon D3s (the most common camera used on the ISS), this response is virtually identical to that of others that have been used, such as the D3, D4 and D5 (Fig. 1).

2. Synthetic photometry

The first thing we need to know in order to use an ISS image to determine the colour of outdoor lighting of an area is to calculate the predicted response of the sensor in the camera to a certain light spectrum. We employ synthetic photometry, a mathematical technique that allows prediction of the spectral features of a light source under different conditions or instrument settings (Straizys, 1996)). This is widely used in astronomy (Fukugita et al., 1995), but can be applied to other photonics based research topics. In astronomy, the brightness of a source, measured in magnitudes, can be predicted based on its spectral energy distribution and that of a reference source as:

$$m_{AB} = -2.5 \log_{10} \frac{\int_0^\infty T(\lambda)\, \phi(\lambda)\, d\lambda}{\int_0^\infty T(\lambda)\, \phi_{ref}(\lambda)\, d\lambda},$$
(1)

where $T(\lambda)$ is the spectral sensitivity of the observation band (including the detector response), $\phi(\lambda)$ is the spectrum of the source and $\phi_{ref}(\lambda)$ a reference spectrum which defines the magnitude system. In particular, for many decades astronomers have employed the spectral energy distribution of the star Vega as a reference. This has not been free from systematic errors due to uncertainties in the absolute flux calibration of this star. For that reason, the tendency at present is to use the so-called AB magnitude system (Oke, 1974), in which the reference spectrum ϕ
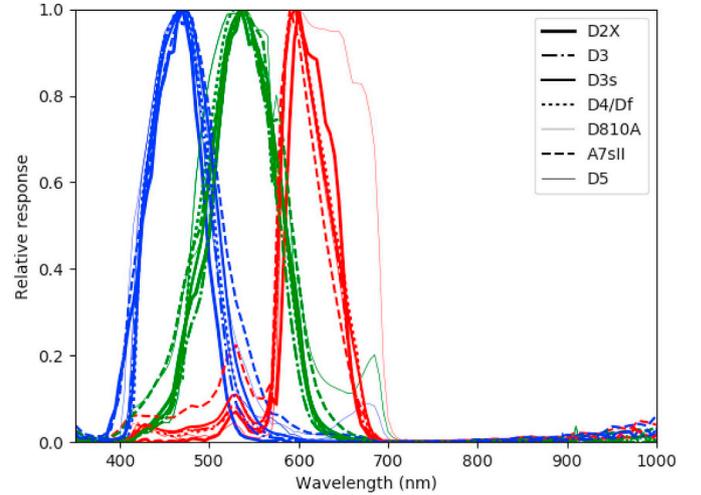
Fig. 1. Spectral responses of recent models of DSLR cameras (Nikon D2X, D3, D3s, D4, D5, Sony A7SII(Sa7SII), Canon5D Mark II(C-5D) and the special astrophotography camera Nikon D810A. All of these cameras, except the D810A and the C-5D, are being (or have been) used on the ISS; the others have been included for comparison. These data were obtained by C. Tapia and A. Sánchez de Miguel at the LICA-UCM laboratory.To facilitate the comparison among responses they have been normalized to a maximum value of 1.

$(\lambda)_{ref} = \phi(\lambda)_{AB}$ does not depend on any particular star but is defined for a source of constant spectral density flux of 3631 Janskys across the spectral range of the band.

In remote sensing, where the AB magnitude system of units is not used, the brightness of a source is quantified as radiance, that can be measured using the much simpler expression:

$$R = \frac{\int_0^\infty T(\lambda)\, \phi(\lambda)\, d\lambda}{\int_0^\infty T(\lambda)\, \phi_{AB}(\lambda)\, d\lambda}.$$
(2)

Conversion from m_{AB}, AB magnitudes, to radiance R can be done using (Sánchez de Miguel et al., 2017):

$$m_{AB} = -2.5 \log_{10}(R) - 5 \log_{10}\bar{\lambda} - 2.41,$$
(3)

where R is expressed in erg s^{-1} $cm^{-2}Å^{-1}$, and $\bar{\lambda}$ is the average wavelength of the band defined by

$$\bar{\lambda} = \frac{\int_0^\infty \lambda\ T(\lambda)\ d\lambda}{\int_0^\infty T(\lambda)\ d\lambda}.$$
(4)

Synthetic photometry measurements can be obtained for any combination of spectral source and wavelength range using Eqs. (1) and (3). In astronomy one can employ the spectrum of many stars for calibration purposes. This is much cheaper, precise and accessible than using absolute calibrated radiometric lamps. In this paper we use radiance ratios of the form:

$$\frac{R}{R'} = \frac{\int_0^\infty T(\lambda)\, \phi(\lambda)\, d\lambda}{\int_0^\infty T'(\lambda)\, \phi(\lambda)\, d\lambda} \frac{\int_0^\infty T'(\lambda)\, \phi(\lambda)_{AB}\, d\lambda}{\int_0^\infty T(\lambda)\, \phi(\lambda)_{AB}\, d\lambda} \equiv C_{T,T'} \frac{\int_0^\infty T(\lambda)\, \phi(\lambda)\, d\lambda}{\int_0^\infty T'(\lambda)\, \phi(\lambda)\, d\lambda},$$
(5)

where R is the radiance in one filter/instrument system, R' is the radiance of the same source using a different filter/instrument system, T and T' are the spectral transmittance of the respective filter/instrument systems, and $C_{T,T'}$ can be considered as a constant after setting the two filter/instrument systems in use. These radiance ratios are called 'colours' in astrophysics and we will use the terms 'colour' and 'ratio' interchangeably.

2.1. Spectral libraries used

In order to predict the colours that will appear on the sensors or the synthetic bands that will be discussed later, it is necessary to have high resolution spectra of the light sources. For this work we have used two different spectral libraries, the LSPDD database and the LICA UCM database. The LSPDD database mainly comprises spectra measured in the laboratory. It includes 254 lamp spectra (with information also about energy efficiency), in ASCII text format (273 nm to 900 nm every 0.5 nm; Sánchez de Miguel et al., 2017). By contrast, the LICA UCM database comprises spectra obtained mainly from measurements made in the field (Tapia et al., 2017). Here we use 50 spectra from this database, mainly for the more common forms of lamps used for street lighting. The two databases complement each other for our purposes since in a laboratory it is difficult to get a real representation of how street light lamps actually perform outside (depending on factors such as changes in spectra due to aging of lamps, frequency of maintenance and cleaning etc.), whilst in the field it is difficult to obtain information on energy efficiency. In this paper we use the classification of illumination technology (kinds of lamps) employed by the LSPDD database. We focus on lamps typical of the street lights of the European Union and Canada, although the industry is constantly creating new kinds of street lights.

3. Lamp classification using RGB DSLR colours

The colour–colour (or two colour) technique has long been used widely in astrophysics to discriminate different light sources based on their predicted physical properties (Öhman, 1949; Dixon, 1965). However, it has not previously been used in the context of nocturnal remote sensing. The technique compares two ratios each of two different bands in a bidimensional space. Each ratio is named as a colour. These colours can be calculated analytically or observed. The large potential of this technique comes from the ease of comparing analytical or theoretical predictions with observations. In our case, we have computed analytically the expected colours (radiance ratios) detected by the camera sensor of a Nikon D3s for the different lamps in the LSPDD and LICA databases using the synthetic photometry technique (see above). DSLR cameras use a Bayer filter in front of the sensor, which comprises microfilters of three different colours, Blue (B), Green (G) and Red (R). With this structure it is possible to obtain for a given field of view four images of three colours simultaneously, one red, one blue and two green images that are identical but from slightly different perspectives. These images do not correspond precisely to the same viewpoint, therefore an interpolation procedure is usually used to obtain a higher resolution image. For the colour–colour technique we use ratios between the colours to obtain a distribution of values on the plane B/G vs G/R. In daylight remote sensing similar techniques have been used for the calculation of the Normalised Difference Vegetation Index (NDVI) since the late 1970s (Rouse Jr et al., 1974; Tucker, 1979; Tucker et al., 2005), although NDVI is a spatial transformation of two bands of a spectral ratio (NIR/VIS), and we propose the use of three bands. For present purposes we assume direct line-of-sight to the light source. In practice, atmospheric corrections may need to be considered when the observation is made from space, or reflectance corrections if the light does not take a direct path to the sensor. We also treat the detector as ideal, so it is not affected by differences in the sensitivity of the camera to different wavelengths or linearity issues. In practice, the RAW image data would also need to be corrected for these effects.

It is important to note that the RAW image is the least processed that a DSLR camera can produce, but whilst in theory this should be completely unprocessed this is usually not the case. Such images do not have corrections for colour balance, linearity corrections, gamma corrections, etc. The JPG format is more common and widespread but this is not the native format and can have several issues. Most JPG images use lossy compression, so a large part of the information is lost. They do
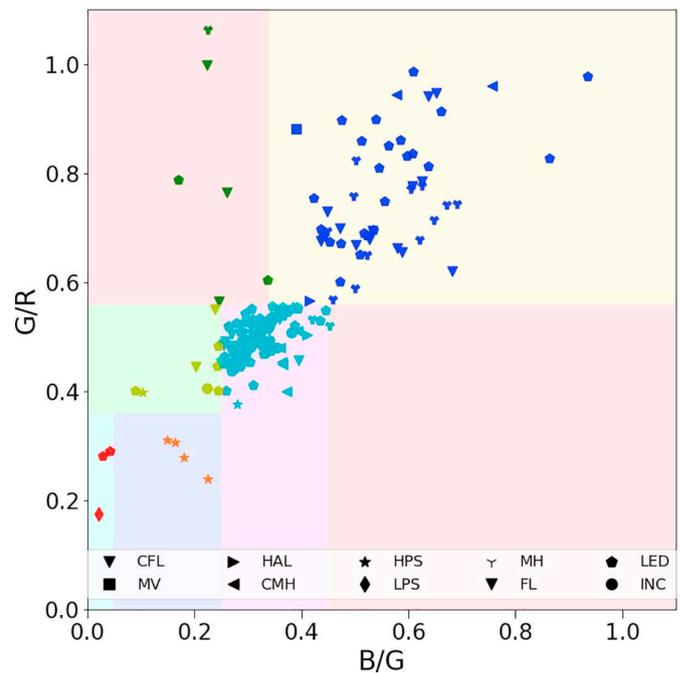
Fig. 2. The distribution of emissions from different kinds of lamps with respect to B/G and G/R ratios. The coloured areas are described in the main text. The colour of the points mimics the colour tone of the lights, so the bluer lamps are coded in dark blue, the reddish in red, etc., with exception of cyan, which represents white lights. The technologies are indicated as HAL - Halogen, MH - Metal Halide, CMH - Ceramic Metal Halide, CFL - Compact Fluorescent, FL - Fluorescent, HPS - High Pressure Sodium, LPS - Low Pressure Sodium, and INC - Incandescent. The symbol used for CFL and FL is the same because they share the same spectral features.

not use the full dynamic range of the data and a gamma correction (Poynton, 1998) is used to make them more human vision friendly, destroying the linearity of the original data. The JPG format is not recommended for quantitative analysis unless all these issues have been addressed first.

Different lamp types do not completely separate out in B/G vs G/R space using the spectral information from the databases (Fig. 2). This said, the likelihood of particular types giving rise to emissions in different regions of this space can be markedly narrowed down. The area framed by B/G [0-0.05] and G/R [0-0.36] can be assigned to Low Pressure Sodium (LPS) and pure amber LEDs; the area B/G [0.05 –0.25] and G/R [0–0.36] to High Pressure Sodium (HPS) light sources; the area B/G [0–0.25] and G/R [0.36 –0.55] has a combination of HPS, LED phosphor converted (PC) amber, some warm light fluorescents, incandescent lamps and other warm LEDs; the area B/G [0.25 –045] and G/R [0–0.55] is where neutral white lamps like LED 3000k and many fluorescents lie; the area B/G [0–0.36] and G/R > 0.55 is where we find lamps with high mercury content, and some LEDs many of which have a greenish colour as a result of degradation from their original specification; the area B/G > 0.36 and G/R > 0.55 has the more bluish lamps like LEDs of 4000k and 5000k, and metal halide lamps. There are also some "forbidden" areas, like the region G/R [0–0.55] and B/G > 0.45, which can only be populated by mixtures of extremely warm lights with extremely cold lights or if there are problems with signal to noise ratios in image data.

4. Evaluation of relationships between environmental measures and RGB colours

Whilst the distribution of lamp types across B/G vs G/R space may not be simple, it may still be the case that one or other of these ratios may show useful relationships with measures of the environmental

impact of artificial nighttime lighting. If this were to be the case, then it would be possible to re-express RGB images taken from the ISS in terms of these measures. Here we evaluate this potential for a varied selection of such measures, namely photopic vision, the Melatonin Suppression Index, the Star Light Index, the Induced Photosynthesis Index, production of NO_2-NO radicals, energy efficiency and CO_2 emissions, and Correlated Colour Temperature.

In each case, we determine the relationships between the measure and the G/R and B/G ratios. The fits reported are statistical approximations. Linear fits were calculated with Robust linear model estimation RANSAC (Pedregosa et al., 2011), in order to reduce the effect of outliers without removing them. Polynomial fits were calculated using the `polyfit` function of Walt et al. (2011). The errors of the fits have been calculated using the bootstrap technique with 1000 iterations and considering one sigma error, so the central value is the median, and data points falling outside the error bars ± 1σ. The selection of the order of the polynomials reported has been decided manually due to the statistical peculiarities of the sample. In particular, whilst some lamp types have an industrial standard single spectrum (and therefore effectively no error in the measurement; e.g. LPS) others have multiple spectra and have been ' field sampled' (with associated error; e.g. LEDs). The reported polynomial fits are those that are judged to give the highest explained variance whilst also not unduly punishing fit to the LPS data because of its representation by only one point.

4.1. Photopic vision

Photopic vision (aka $V(\lambda)$ or luminance) is that which humans use when illumination levels are higher than $\sim 0.7 cd/m^2$ (Eloholma and Halonen, 2006). There is a strong relationship between the ratio G/R and the $V(\lambda)$/G ratio derived from the sensitivity curve for this vision (Smith and Guild, 1931) (Table 1, Fig. 3). The relationship is not linear,

Table 1
Relationships between different environmental indices and the G/R or B/G ratios obtained from imagery from a DSLR. In all cases the number of spectra used is 206. $f(x)$ indicates the function where x is equal to B/G or G/R. Factors represent the p_n values of the polynomial fit. Uncertainties in the coefficients are given as ± δ. Valid area represents the X range where the fit is accurate.

Relationship	Factors ($p_n \cdot x^n + ... + p_0 \cdot x^0$)	Valid area(x)	R^2	p value
Photopic				
$V(\lambda)/G = f(G/R)$	− 4.0 + 9.8 − 8.2 + 3.60	[0.1,1.1]	0.97	< 0.001
− δ	− 0.5 − 0.6 − 0.5 − 0.06			
+ δ	+ 0.4 + 0.9 + 0.3 + 0.09			
$V(\lambda)/G = f(B/G)$	− 2.4 + 4.9 − 3.6 + 2.15	[0.0,1.0]	0.72	< 0.001
− δ	− 1.2 − 1.8 − 0.8 − 0.13			
+ δ	+ 1.1 + 1.8 + 0.8 + 0.12			
Melatonin Suppression Index				
$MSI = f(B/G)$	+ 1.09 − 0.053	[0.15,1.0]	0.87	< 0.001
− δ	− 0.05 − 0.019			
+ δ	+ 0.05 + 0.019			
$MSI = f(G/R)$	0.97 − 0.19	[0.0,1.0]	0.68	< 0.001
− δ	− 0.12 − 0.06			
+ δ	+ 0.12 + 0.06			
$msas/G = f(B/G)$	+ 0.75 + 0.03	[0.0,0.8]	0.88	< 0.001
− δ	− 0.02 − 0.01			
+ δ	+ 0.03 + 0.01			
$msas/G = f(G/R)$	+ 0.57 − 0.02	[0.18,1.0]	0.54	< 0.001
− δ	− 0.06 − 0.04			
+ δ	+ 0.08 + 0.03			
Stellar Light Index				
$SLI = f(G/R)$	+ 0.84 + 0.07	[0.18,1.0]	0.64	< 0.001
− δ	− 0.18 − 0.09			
+ δ	+ 0.18 + 0.09			
$SLI = f(B/G)$	+ 0.59 + 0.14	[0.0,0.8]	0.84	< 0.001
− δ	− 0.04 − 0.08			
+ δ	+ 0.03 + 0.12			

such that errors in the determination of lower values of the G/R ratio will lead to larger errors in the $V(\lambda)$/G ratio. This relationship can nonetheless be very useful to convert images taken by DSLRs to units of Lux or Candelas that are used in most regulations concerning artificial lighting. Assuming that radiation is monochromatic, radiometric units of Watts per steradian can be converted to Candelas by dividing by 683 (Zong, 2016). However, we do not recommend use of this conversion in remote sensing applications if the spatial resolution of the image is less than m /pixel. If the resolution of the image is higher than m /pixel, this can be used for a reliable measure of illumination, that can have legal implications. This is because these units are usually used to measure illumination for regulatory purposes. Values measured at low spatial resolution will be misleading because they will include illuminance from a mixture of surfaces, including the roofs of buildings. In order for the end result to represent photopic intensity we need to multiply the intensity of the green channel V(λ)/G ratio (Eq. (6)) (this paper):

$$V(\lambda) = V(\lambda)/G \ (B/G \ or \ G/R) \cdot G \tag{6}$$

This equation gives us the possibility of measuring luminance using DSLR cameras, by getting an estimate of the $V(\lambda)$/G ratio from B/G or G/R ratio images and the intensity on the G channel.

4.2. Melatonin Suppression Index and Melatonin Suppression band

Melatonin is one of the key drivers of biological rhythms in a wide array of organisms, and its production is highly responsive to light spectra. The Melatonin Suppression Index was defined by Aubé et al. (2013) using the melanopsin response function (aka msas) published by Thapan et al. (2001) and Brainard et al. (2001). The MSI values are weighted by photopic intensity and constitute a measure of the potential suppression of melatonin production by a light source compared to the solar spectrum:

$$MSI = \frac{\int_{380nm}^{730nm} \phi_n(lamp)(r, \lambda) M(\lambda) d\lambda}{\int_{380nm}^{730nm} \phi_n(D65))(r, \lambda) M(\lambda) d\lambda} \tag{7}$$

There is a linear relationship between MSI and the G/R ratio (Table 1, Fig. 4). The dispersion of values is greater for bluer lamp sources. However, for most lamps this relationship is sufficient for an estimate of MSI of better than $^{+0.2}_{-0.05}$, data points falling outside the error bars, that allow us to estimate the MSI of the sources with a typical precision of 75%. There is a tighter linear relationship between MSI and the B/G ratio (Table 1, Fig. 4), although it is much more difficult to get a good signal to noise ratio on the blue channel of DSLRs than on the green and red. Using both relationships, we can obtain a more reliable estimate of the real MSI value. MSI is weighted by the human vision response, so that we can measure with the $V(\lambda)$/G relationship we can calculate the real impact by the next equation (this paper):

$$MSI \ Impact = MSI(B/G \ or \ G/R) \cdot \left[\frac{V(\lambda)}{G}(B/G \ or \ G/R) \right] \cdot G \tag{8}$$

Sometimes we might want to skip the step of the estimation of luminance (aka V(λ)) and go directly to estimate the energy emitted across the melatonin suppression band (msas). Indeed, this variable shows less scattered relationships with G/R and B/G ratios, but it is not weighted by the human vision response (Fig. 5).

$$msas \ intensity = msas/G \ (B/G \ or \ G/R) \cdot G \tag{9}$$

If we want to know the total intensity emitted in the melatonin suppression band we need to apply Eq. (9) (this paper). Doing so allows the intensive function of msas/G and extensive values of a G image to be combined. As msas/G ratio is a function of B/G or G/R spectral values it is possible to create images that represent msas/G by using B/G or G/R images.

The potential application of this or derived indicators can be appreciated from recent publication of the finding of a statistically
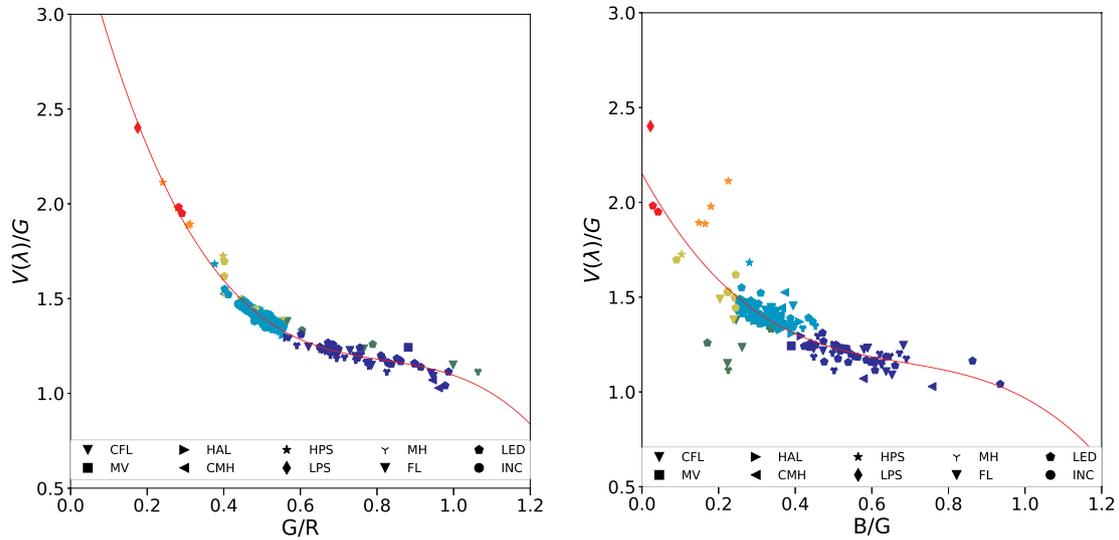
Fig. 3. Relationship between photopic vision and (left) the G/R ratio and (right) the B/G ratio. Colours are the same as in Fig. 2.

significant correlation between MSI and the risks of breast and prostate cancer (Garcia-Saenz et al., 2018).

4.3. Star Light Index and Scotopic vision

The loss of visibility of stars as a consequence of artificial nighttime lighting is a particular concern to astronomers, but may have wider impacts in terms of limiting human experiences of the natural world (Kyba, 2018) and nocturnal orientation by other species (Bird and Parker, 2014; Wallraff, 1960; Warrant and Dacke, 2011). The Star Light Index (SLI) was defined by Aubé et al. (2013) using human scotopic vision (CIE 1951; Wyszecki and Stiles (1982)) aka $V'(\lambda)$, as a measure of the visibility of stars to people:

$$SLI = \frac{\int_{380nm}^{730nm} \phi_n(lamp)(r, \lambda)S(\lambda)d\lambda}{\int_{380nm}^{730nm} \phi_n(D65))(r, \lambda)S(\lambda)d\lambda} \quad (10)$$

There is a polynomial relationship between SLI and the G/R ratio (Table 1, Fig. 6). Similar to MSI, the blueish light sources are more dispersed than the warm light sources. In addition, the plot shows a good fit concerning the predicted SLI values derived from the spectra using the B/G ratio (Table 1). This SLI(B/G)relationship is less scattered than the SLI(G/R) ratio, although the level of accuracy will depend on the signal to noise ratio. Usually, the blue channel has a lower signal to noise ratio. Therefore, the G/R relationship will often be more accurate. Similar to how we obtained the actual photopic intensity, in order for us to obtain the scotopic intensity we also calculated the $V'(\lambda)/G$ using the B/G and G/R ratios and the G channel (Fig. 7). In other words, the equation used for obtaining the photopic intensity can also be applied to obtain the scotopic intensity simply by replacing the $V(\lambda)/G$ function with the $V'(\lambda)/G$ function. In addition, by joining these two functions we are also able to estimate the scotopic-photopic (SP) ratio. The SP ratio is useful for determining the impact on star visibility. It should be noted that, contrary to the belief of some researchers, the SP ratio is not useful for establishing suitable illumination intensity levels since scotopic vision starts at 0.5 lx. This means that scotopic vision is used only when illumination intensity levels are extremely low. Much lower than the average lit street.
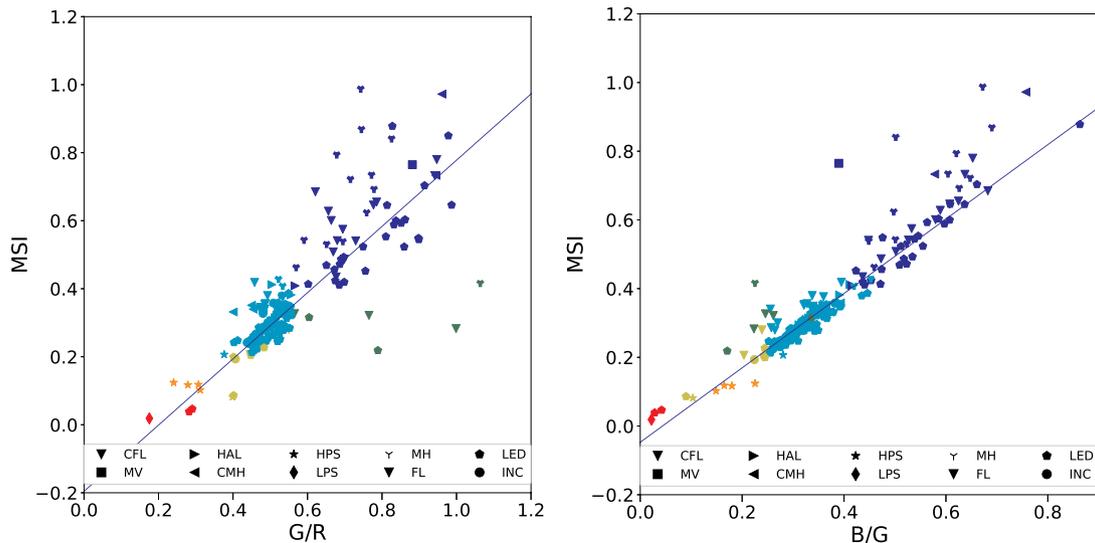
Fig. 4. Relationship between the Melatonin Suppression Index (MSI) and (left) the G/R ratio and (right) the B/G ratio. Colours are the same as in Fig. 2.
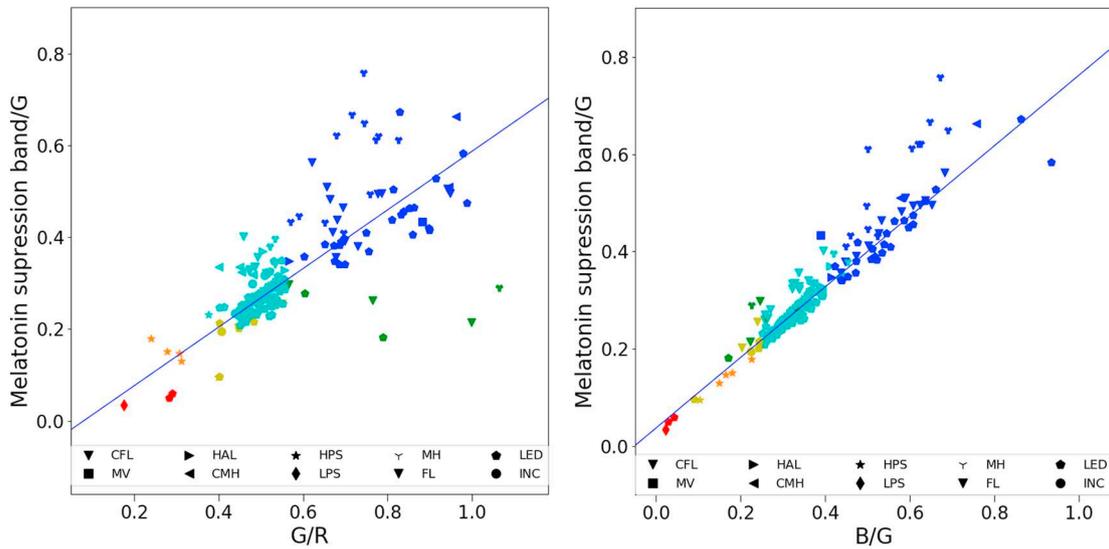
Fig. 5. Relationship between the Melatonin Suppression band and Green band ratio and (left) the B/G ratio and (right) the G/R ratio. Colours are the same as in Fig. 2.

4.4. Induced Photosynthesis Index and Photosynthetic band

The Induced Photosynthesis Index (IPI) has been defined by Aubé et al. (2013) using Germany: Deutsches Institut Fur Normung EV (German National Standard) (2000), and represents the potential of a source of illumination to enable plant photosynthesis.

$$IPI = \frac{\int_{380nm}^{730nm} \phi_n(lamp)(r, \lambda) I(\lambda) d\lambda}{\int_{380nm}^{730nm} \phi_n(lamp))(r, \lambda) I(\lambda) d\lambda} \quad (11)$$

There is no relationship between the IPI and the G/R ratio (see in supplementary materials) or the B/G ratio (Table 2). We conclude that as the spectral sensitivity of photosynthesis is so broad, any lamp spectrum, no matter the dominant wavelengths, can produce a photosynthetic response. The highest response is to lamps that have emissions similar to a black body (this is logical as plants are adapted to respond

to sunlight that is effectively emission from a black body). There is not a significant correlation between the IPI and the ratio G/R, and more careful analysis is needed to exclude the black bodies (Fig. 8).

4.5. Production of NO₂-NO radicals

Stark et al. (2011) observed that emissions from city lights can interact with the chemistry of the atmospheric production of NO_2 and NO radicals and thus change levels of air pollution, with different types of lamps influencing this interaction differently.

$$\frac{j(NO_3)}{Luminance} = \frac{\int \phi_n(lamp)(r, \lambda) \sigma_{NO_3}(\lambda) \cdot [\phi_{NO_3 \to NO_2}(\lambda) + \phi_{NO_3 \to NO}(\lambda)] d\lambda}{\int \phi_n(lamp)(r, \lambda) V(\lambda) d\lambda} \quad (12)$$

Because of the complicated absorption spectrum of NO_3 (aka jNO_3), the main precursor of NO_2 and NO, it does not show a good relationship
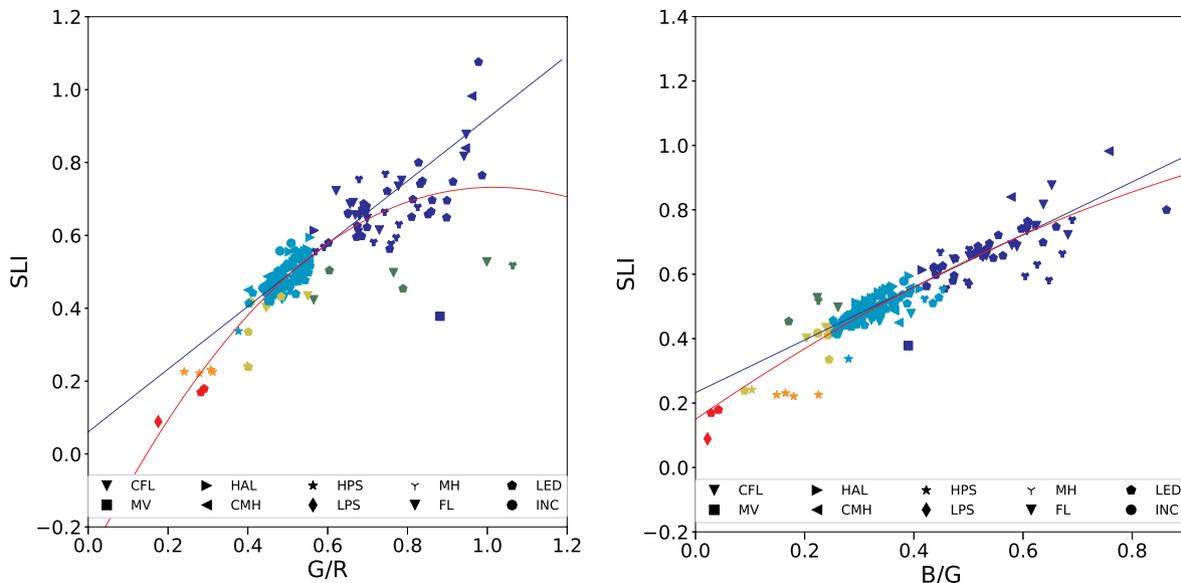
Fig. 6. Relationship between the Stellar light Index and (left) the G/R ratio and (right) the B/G ratio, with linear (blue) and polynomial fits (red). Colours are the same as in Fig. 2.
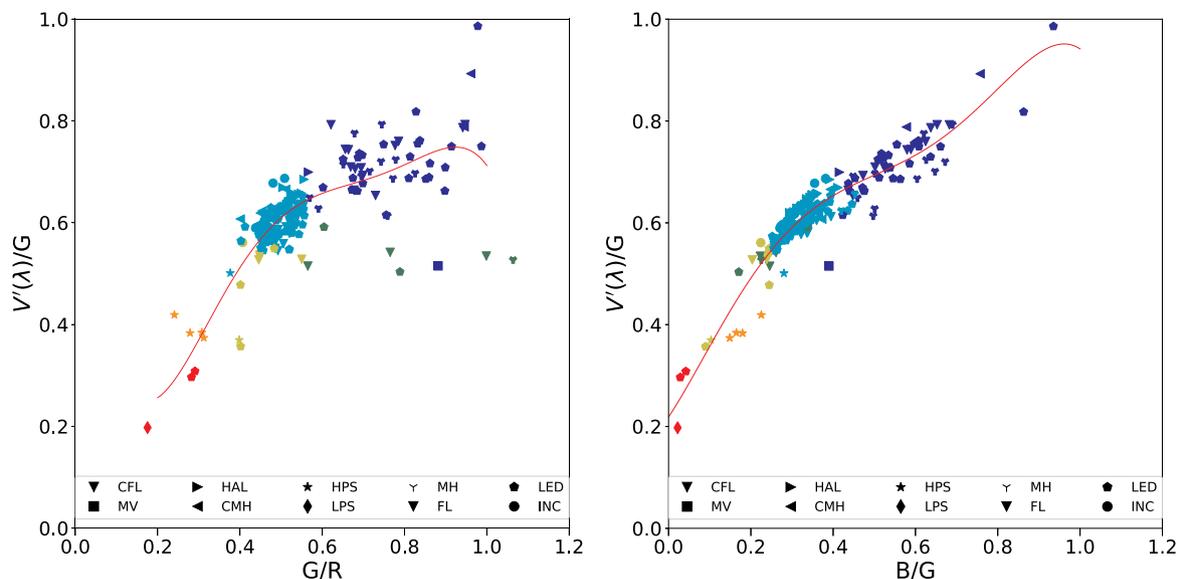
Fig. 7. Relationship between Scotopic vision and G band ratio and (left) the G/R ratio and (right) the B/G ratio. Colours are the same as in Fig. 2.

with the G/R ratio (Fig. 9, Table 2) nor with the B/G ratio (Table 2). However, LPS lamps are associated with much higher levels of yields of NO_3 than are other lamps. Eq. (12) is the formula used to create Fig. 9, more details in Stark et al. (2011).

4.6. Energy efficiency - CO2 production

There is much interest in estimating the energy efficiency of lighting - which has obvious implications for its wider environmental impacts - and how this is changing, at landscape scales and above (e.g.

nationally). However, there is no relationship between luminous efficacy measures of lamps from the LSPDD database or from Wikipedia contributors (2018) and either the G/R ratio or the B/G ratio when considering all the lighting technologies (Table 2). Some authors have argued that there is a correlation at higher levels of Correlated Colour Temperature (for definition see below) (Donatello et al., 2017). However, we found no marked relationship amongst just the white light technologies. In short, there is no way to determine energy efficiency using only the colour of lights without knowledge of the technology that is producing this specific colour, and even in that case for some

Table 2

Relationships between different environmental indices and the G/R or B/G ratios obtained from imagery from a DSLR. In all cases the number of spectra used is 206. *f* (*X*) indicates the function where x is equal to B/G or G/R. Factors represent the p_n values of the polynomial fit. Uncertainties in the coefficients are given as ± *δ*. Valid area represents the *X* range where the fit is accurate.

Relationship	Factors ($p_n \cdot x^n + \dots + p_0 \cdot x^0$)	Valid area(x)	R^2	p value
Scotopic vision				
$V'(\lambda)/G = f(G/R)$	− 27 + 81 − 91 + 47 − 9 + 0.9	[0.18,0.9]	0.66	< 0.001
− *δ*	− 18 − 65 − 80 − 37 − 15 − 0.8			
+ *δ*	+ 22 + 63 + 72 + 50 + 9 + 1.8			
$V'(\lambda)/G = f(B/G)$	− 15 + 33 − 25 + 6 + 0.7 + 0.23	[0.0,1.0]	0.90	< 0.001
− *δ*	− 15 − 26 − 25 − 7 − 1.1 − 0.05			
+ *δ*	+ 12 + 32 + 21 + 8 + 1.1 + 0.05			
Induced Photosynthesis Index				
IPI = f (B/G) no fit	NO		NO	NO
IPI = f (G/R) no fit	NO		NO	NO
Correlated Color Temperature				
$CCT = 10^4 \cdot f(G/R)$	− 3.0 + 5.8 − 3.2 + 1.0 + 0.06	[0.2,1.]	0.91	< 0.001
− *δ*	− 1.5 − 4.3 − 3.5 − 1.2 − 0.14			
+ *δ*	+ 1.5 + 3.8 + 3.5 + 1.1 + 0.14			
$CCT = 10^4 \cdot f(B/G)$	− 3.6 + 6.0 − 1.6 + 0.4 + 0.18	[0,1]	0.82	< 0.001
− *δ*	− 4.0 − 4.6 − 3.3 − 0.5 − 0.03			
+ *δ*	+ 2.6 + 6.2 + 2.6 + 0.6 + 0.03			
Yields NO3				
jNO3/V(λ) = f (B/G) no fit	NO		0.38	NO
jNO3/V(λ) = f (G/R) no fit	NO		0.008	NO
Luminosity efficiency				
Lum. eff. = f(G/R) no fit	NO		NO	NO
Lum. eff. = f(B/G) no fit	NO		NO	NO
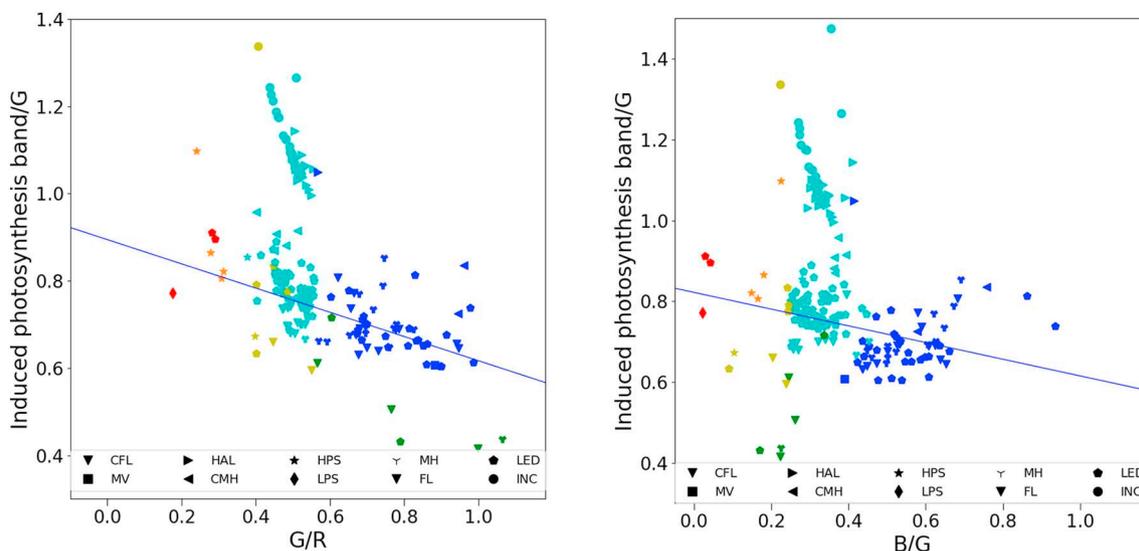
Fig. 8. Relationship between the Induced Photosynthesis band and G ratio and (left) the G/R ratio and (right) the B/G ratio. Colours are the same as in Fig. 2.

technologies, such as LEDs, a wide range of energy efficiencies is possible.

4.7. Correlated Colour Temperature

Correlated Colour Temperature (CCT) is a measure of the human sensation of colour compared with black bodies of a certain temperature (McCamy, 1992). This parameter is widely used by the lighting industry and in photography to give an approximate sense of the colour of light, although it poorly captures the blue content of light sources, which is a significant issue with regard to many "white" LEDs (Galadí-Enríquez, 2018). CCT and the G/R ratio are related in an approximately linear fashion (Fig. 10), but the best fit is a polynomial one. The scatter is much greater for bluer lamps. CCT has been criticized because it does not represent the environmental impact of the light, even though it has been used in several regulations that are intended to do so (Kinzey et al., 2017).

5. Milan an example application

Probably the best known recent conversion of a streetlight system has been in 2015 in the city of Milan during which high pressure sodium lamps were replaced with LEDs. In this section we use nighttime images from the ISS taken before and after this conversion as an example of the application of the methodology described in this paper. The images used are ISS032-e-012145(2012) and ISS043-e-093509(2015) taken from Sánchez de Miguel et al. (2015) and downloaded from NASA's Gateway to Astronaut Photography of Earth (https://eol.jsc.nasa.gov/).

To apply the statistical relationships between the RGB values and the environmental variables it is necessary to make several corrections to the raw image data of the city since this does not represent the real intensity of the RGB channels. Neither does the raw data show the real ratios between the different channels. In order to resolve these discrepancies we applied standard procedures of decodification of the raw
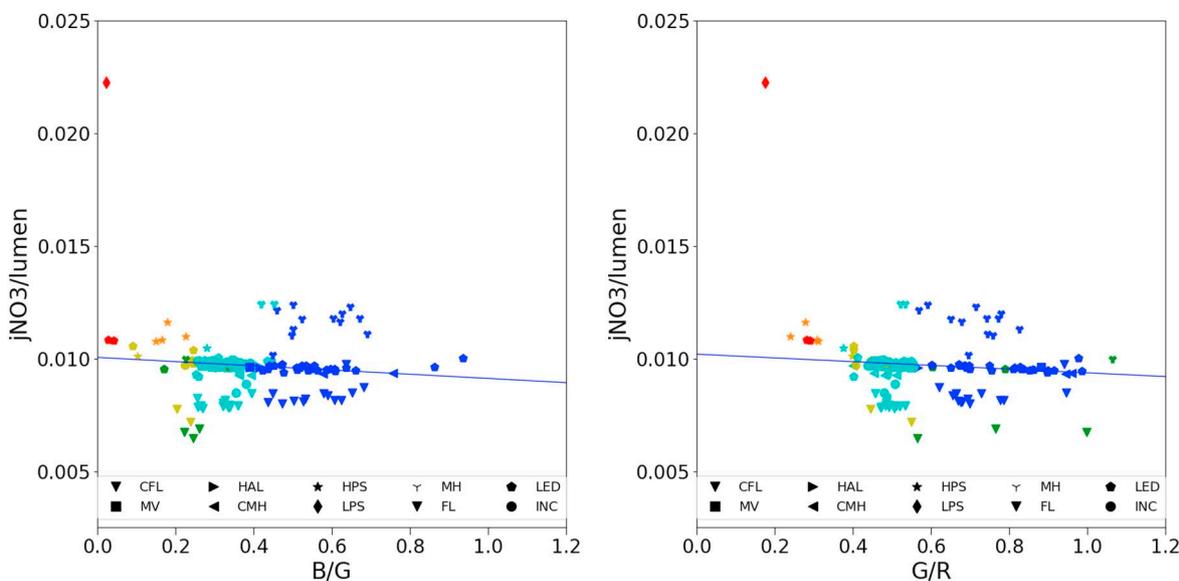
Fig. 9. Relationship between $NO_2 + NO$ radical production and (left) the B/G ratio and (right) the G/R ratio. Colours are the same as in Fig. 2.
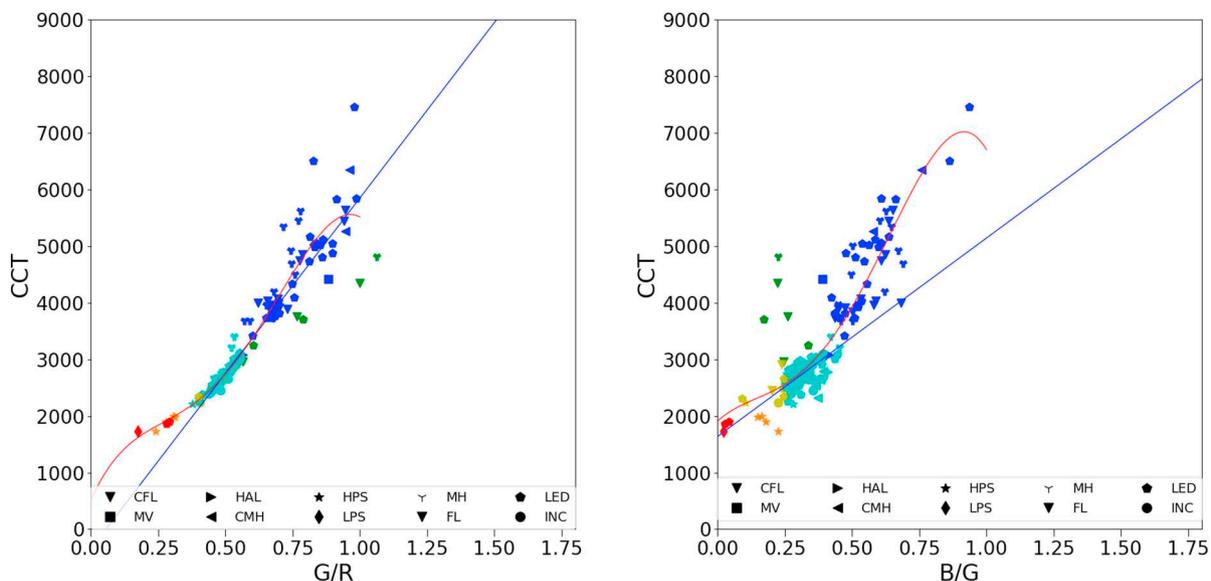
Fig. 10. Relationship between Correlated Colour Temperature (CCT) and (left) the G/R ratio and (right) the B/G ratio, with linear (blue) and polynomial fits (red). Colours are the same as in Fig. 2.

data, linearity correction of the sensor and vignetting correction of the lens (Sánchez de Miguel, 2015). Furthermore, corrections of the relative intensity between channels have been applied. For accuracy, calibrations used the same lens and camera models used by the astronauts to take the images. Because, we are using the images for a comparative analysis only, we did not need to apply atmospheric corrections or ISS window transmission corrections.

We focus on two of the environmental measures, photopic intensity and MSI. There was no measurable change in photopic intensity, estimated using Eq. (6), across Milan between the two time periods
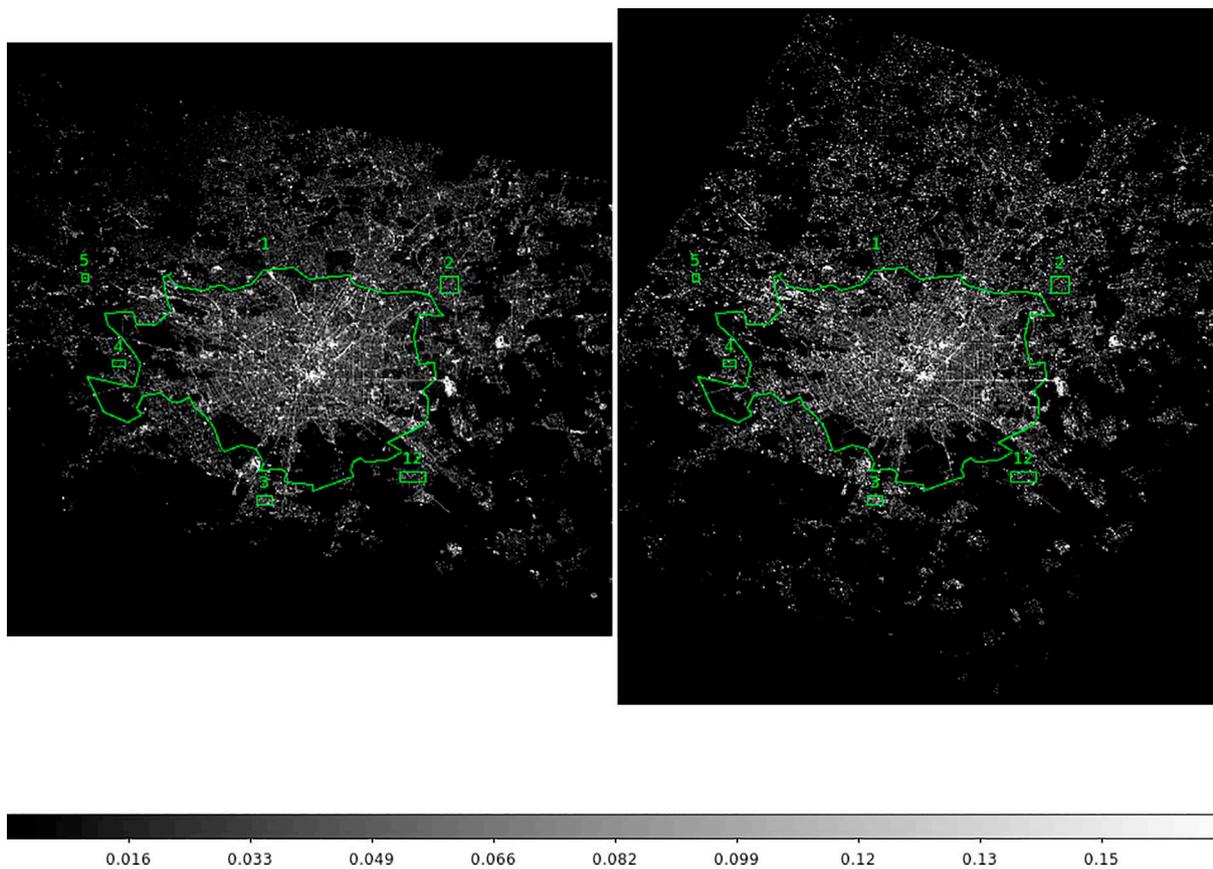
Fig. 11. Images taken from the ISS corrected to represent photopic intensity (units proportional to lux). Milan in 2012 (left) and in 2015 (right). The green rectangles are the reference regions for the differential photometry, and the polygon represents the municipality of Milan.
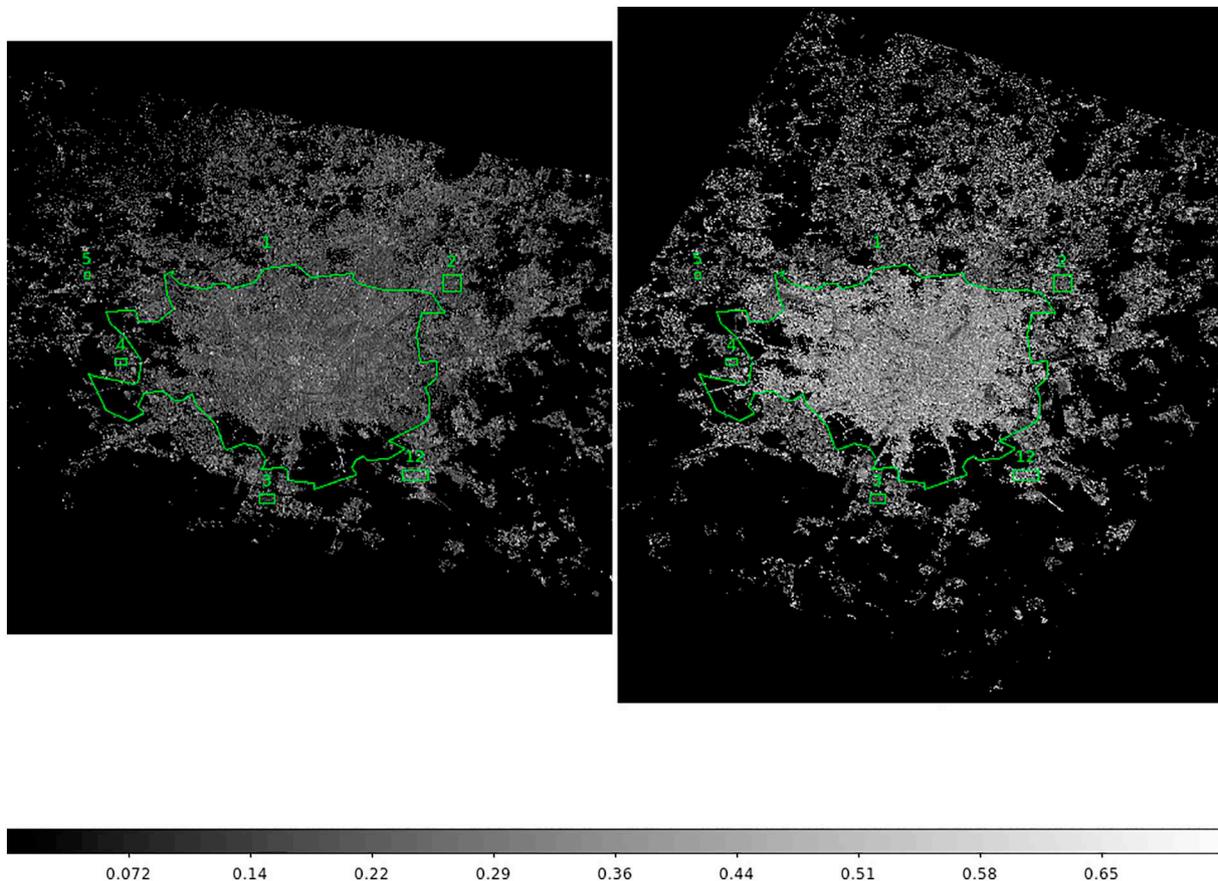
Fig. 12. Images taken from the ISS corrected to represent MSI. Milan in 2012 (left) and in 2015 (right). Rectangles and polygon as in Fig. 11.

(Fig. 11; measured variation was 0% 5%). This makes sense because the streetlight conversion was designed to produce the same luminance level as did the original streetlights. By contrast, there was an increase in values of MSI, estimated using Eq. (7), of 37% in Milan (Fig. 12). Weighting MSI by photopic vision, using Eq. (8), shows an increase of 23% (Fig. 13).

6. Discussion

Images of the Earth taken using DSLR cameras from the ISS, and potentially other platforms, can provide valuable data on the colour of nighttime artificial lighting. As reported here, we have determined an approach to extracting these data through the use of colour-colour diagrams. In turn, this enables the association to be determined with a variety of measures of environmental impacts (Tables 1 and 2). In some cases these relationships are strong (e.g. Photopic vision, Melatonin Suppression Index), providing a basis for creating spatial maps of potential risks of artificial lighting and also how those risks are changing through time. In other cases these relationships are poor or non-existent (e.g. Induced Photosynthesis Index, energy efficiency), meaning that such maps cannot be created.

This method is analytical, and uses calculations of the light spectra to determine the lamp colours. The important advantage of this approach is that it is device independent. And therefore, the cameras should be calibrated to fit the predicted colours. This means that success or failure "only" depends on the signal to noise ratio as well as the accurate characterisation of the DSLR cameras, the completeness of the spectral databases and other environmental corrections. The only limitation of this method is that, although the data concerning predicted colours is fully reliable, some field study is needed in order to set initial accurate boundaries for the clusters of predicted colours. This

additional data will allow for precise fine tuning devices used in studies. We propose that the radiance calibrated G/R and B/G ratios be termed the Normalized Ratio Light Index (NRLI) Warm and Cold respectively, that is NRLIw and NRLIc, to distinguish them from non-radiance calibrated G/R and B/G ratios used by other authors (Hale et al., 2013).

Whilst our focus is on the potential for using the method documented here to measure the environmental impacts of artificial nighttime lighting using images taken from the ISS, the approach is applicable to DSLR camera images from other platforms. Terrestrial-based and airborne images of cities at night could be useful tools to assess the environmental impacts of artificial light, particularly in assessing historical changes where new measurements are not possible. Field ecological studies on the impacts of artificial light on ecosystems often lack a spectral characterisation of light sources due to the cost of spectrophotometers, despite the importance of emission spectra for the ecological responses (Bennie et al., 2016; Davies et al., 2017); the routine use of DSLR images could help to fill this gap.

A recent conservative approach, that is limited because of the spectral range of the VIIRS satellite sensor (Hillger et al., 2013; Miller et al., 2012), has estimated that both the extent and intensity of artificial nighttime lighting are growing globally at a rate of about 2% per annum (Kyba et al., 2017). Perhaps more significantly, the rate of increase is similar across regions that, over the time period analysed (2012–2016), began with very different levels of artificial lighting. Thus the environmental pressures that result from the introduction of lighting (see Section 1) are both being introduced into areas in which previously they have not been experienced, and are being exacerbated in regions in which they may already have been quite acute. Given that these pressures are sensitive to the spectrum of lighting, having tools to track the spatial pattern and change in this spectrum will be vital.
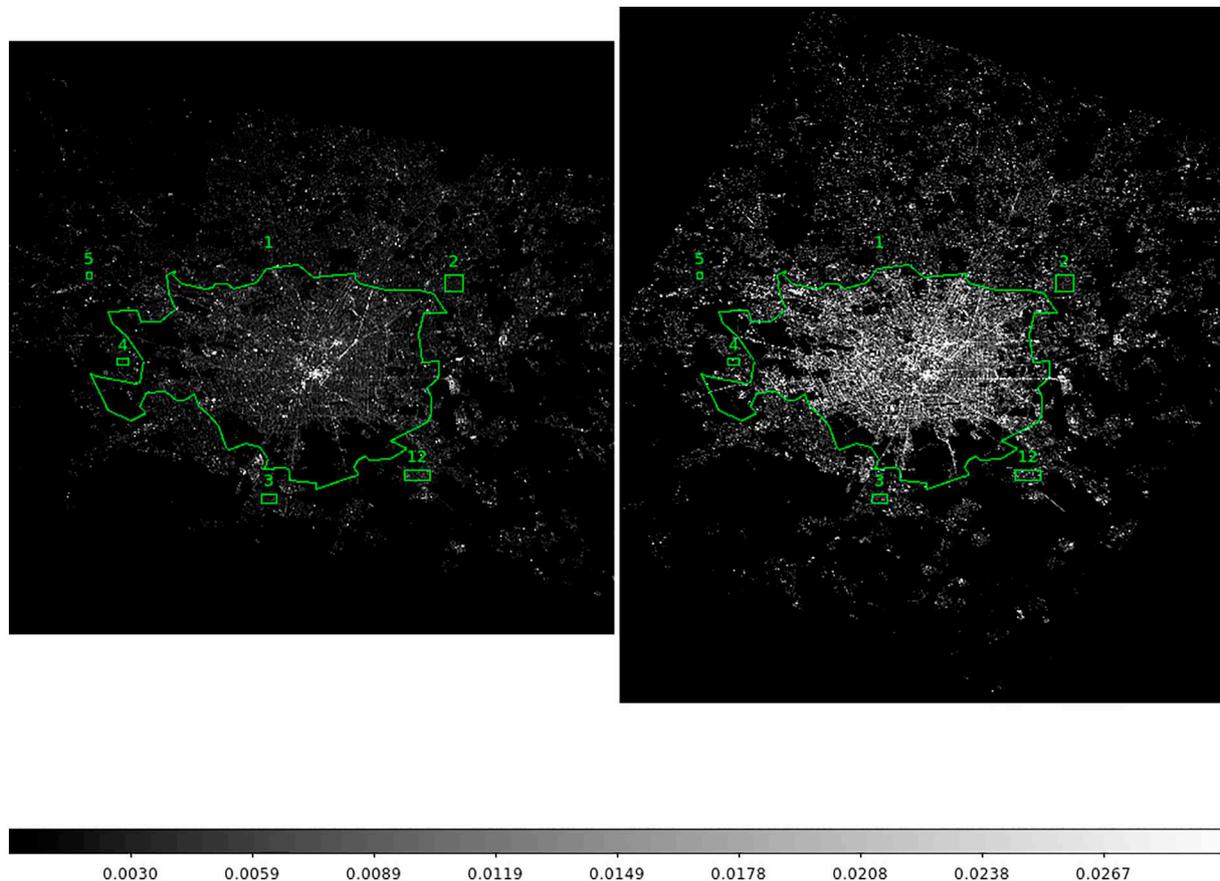
Fig. 13. Images taken from the ISS corrected to represent the impact on MSI. It shows weighted MSI by photopic vision, using Eq. (8). Milan in 2012 (left) and in 2015 (right). Rectangles and polygon as in Fig. 11.

Acknowledgements

Appendix A. Supplementary data

Supplementary data to this article can be found online at https://doi.org/10.1016/j.rse.2019.01.035.

References

Altermatt, F., Ebert, D., 2016. Reduced flight-to-light behaviour of moth populations exposed to long-term urban light pollution. Biol. Lett. 12, 20160111.

Aubé, M., Roby, J., Kocifaj, M., 2013. Evaluating potential spectral impacts of various artificial lights on melatonin suppression, photosynthesis, and star visibility. PloS One 8, e67798.

Bennie, J., Davies, T.W., Cruse, D., Gaston, K.J., 2016. Ecological effects of artificial light at night on wild plants. J. Ecol. 104, 611–620.

Bird, S., Parker, J., 2014. Low levels of light pollution may block the ability of male glow-worms (*Lampyris noctiluca* l.) to locate females. J. Insect Conserv. 18, 737–743.

Brainard, G.C., Hanifin, J.P., Greeson, J.M., Byrne, B., Glickman, G., Gerner, E., Rollag, M.D., 2001. Action spectrum for melatonin regulation in humans: evidence for a novel circadian photoreceptor. J. Neurosci. 21, 6405–6412.

Carr, J., Liu, X., Baker, B., Chance, K., 2017. Observing nightlights from space with tempo. Int. J. Sustain. Light. 19, 26–35.

Davies, T.W., Bennie, J., Cruse, D., Blumgart, D., Inger, R., Gaston, K.J., 2017. Multiple night-time light-emitting diode lighting strategies impact grassland invertebrate assemblages. Glob. Chang. Biol. 23, 2641–2648.

Davies, T.W., Bennie, J., Inger, R., Ibarra, N.H., Gaston, K.J., 2013. Artificial light pollution: are shifting spectral signatures changing the balance of species interactions? Glob. Chang. Biol. 19, 1417–1423.

Davies, T.W., Duffy, J.P., Bennie, J., Gaston, K.J., 2014. The nature, extent, and ecological implications of marine light pollution. Front. Ecol. Environ. 12, 347–355.

Dixon, M.E., 1965. The two-colour diagram as a key to past rates of star formation and past rates of maetal enrichment of the interstellar medium. Mon. Not. R. Astron. Soc. 129, 51–61.

Dominoni, D., Quetting, M., Partecke, J., 2013. Artificial light at night advances avian reproductive physiology. Proc. R. Soc. B 280, 20123017.

Donatello, S., Traverso, M., Rodríguez Quintero, R., Gama Caldas, M., Wolf, O., Van Tichelen, P., Van Hoof, V., Geerken, T., 2017. Technical report and criteria proposal (2nd draft). In: Revision of the EU Green Public Procurement Criteria for Road Lighting.

Dwyer, R.G., Bearhop, S., Campbell, H.A., Bryant, D.M., 2013. Shedding light on light: benefits of anthropogenic illumination to a nocturnally foraging shorebird. J. Anim. Ecol. 82, 478–485.

Eloholma, M., Halonen, L., 2006. New model for mesopic photometry and its application to road lighting. Leukos 2, 263–293.

Elvidge, C.D., Baugh, K.E., Dietz, J.B., Bland, T., Sutton, P.C., Kroehl, H.W., 1999. Radiance calibration of DMSP-OLS low-light imaging data of human settlements. Remote Sens. Environ. 68, 77–88.

Elvidge, C.D., Cinzano, P., Pettit, D.R., Arvesen, J., Sutton, P., Small, C., Nemani, R., Longcore, T., Rich, C., Safran, J., Weeks, J., Ebener, S., 2007. The nightsat mission

concept. Int. J. Remote Sens. 28, 2645–2670.

Elvidge, C.D., Keith, D.M., Tuttle, B.T., Baugh, K.E., 2010. Spectral identification of lighting type and character. Sensors 10, 3961–3988.

Fukugita, M., Shimasaku, K., Ichikawa, T., 1995. Galaxy colors in various photometric band systems. Publ. Astron. Soc. Pac. 107, 945.

Galadí-Enríquez, D., 2018. Beyond CCT: the spectral index system as a tool for the objective, quantitative characterization of lamps. J. Quant. Spectrosc. Radiat. Transf. 206, 399–408.

Garcia-Saenz, A., de Miguel, A.S., Espinosa, A., Valentin, A., Aragonés, N., Llorca, J., Amiano, P., Sánchez, V.M., Guevara, M., Capelo, R., et al., 2018. Evaluating the association between artificial light-at-night exposure and breast and prostate cancer risk in Spain (MCC-Spain study). Environ. Health Perspect. (Online) 126.

Gaston, K.J., Bennie, J., 2014. Demographic effects of artificial nighttime lighting on animal populations. Environ. Rev. 22, 323–330.

Gaston, K.J., Duffy, J.P., Gaston, S., Bennie, J., Davies, T.W., 2014. Human alteration of natural light cycles: causes and ecological consequences. Oecologia 176, 917–931.

Germany: Deutsches Institut Fur Normung EV (German National Standard), 2000. DIN 5031-10, Optical Radiation Physics and Illuminating Engineering - Part 10: Photobiologically Effective Radiation, Quantities, Symbols and Action Spectra.DIN 5031-10, Optical Radiation Physics and Illuminating Engineering - Part 10: Photobiologically Effective Radiation, Quantities, Symbols and Action Spectra.

Hale, J.D., Davies, G., Fairbrass, A.J., Matthews, T.J., Rogers, C.D., Sadler, J.P., 2013. Mapping lightscapes: spatial patterning of artificial lighting in an urban landscape. PloS One 8, e61460.

Hillger, D., Kopp, T., Lee, T., Lindsey, D., Seaman, C., Miller, S., Solbrig, J., Kidder, S., Bachmeier, S., Jasmin, T., et al., 2013. First-light imagery from Suomi NPP VIIRS. Bull. Am. Meteorol. Soc. 94, 1019–1029.

Hölker, F., Wurzbacher, C., Weißenborn, C., Monaghan, M.T., Holzhauer, S.I., Premke, K., 2015. Microbial diversity and community respiration in freshwater sediments influenced by artificial light at night. Philos. Trans. R. Soc. B 370, 20140130.

Kinzey, B., Perrin, T.E., Miller, N.J., Kocifaj, M., Aubé, M., Lamphar, H.S., 2017. An Investigation of LED Street Lighting's Impact on Sky Glow.

Kuechly, H.U., Kyba, C.C.M., Ruhtz, T., Lindemann, C., Wolter, C., Fischer, J., Hölker, F., 2012. Aerial survey of light pollution in Berlin, Germany, and spatial analysis of sources. Remote Sens. Environ. 126, 39–50.

Kyba, C., Garz, S., Kuechly, H., Sánchez de Miguel, A., Zamorano, J., Fischer, J., Hölker, F., 2014. High-resolution imagery of earth at night: new sources, opportunities and challenges. Remote Sens. 7, 1–23.

Kyba, C.C., 2018. Is light pollution getting better or worse? Nat. Astron. 2, 267.

Kyba, C.C., Kuester, T., Sánchez de Miguel, A., Baugh, K., Jechow, A., Hölker, F., Bennie, J., Elvidge, C.D., Gaston, K.J., Guanter, L., 2017. Artificially lit surface of earth at night increasing in radiance and extent. Sci. Adv. 3, e1701528.

Levin, N., Johansen, K., Hacker, J.M., Phinn, S., 2014. A new source for high spatial resolution night time images-the EROS-B commercial satellite. Remote Sens. Environ. 149, 1–12.

Liao, L., Weiss, S., Mills, S., Hauss, B., 2013. Suomi NPP VIIRS day-night band on-orbit performance. J. Geophys. Res.: Atmos. 118.

McCamy, C.S., 1992. Correlated color temperature as an explicit function of chromaticity coordinates. Color Res. Appl. 17, 142–144.

Metcalf, J.P., 2012. Detecting and characterizing nighttime lighting using multispectral and hyperspectral imaging. Ph.D. thesis. Monterey, California. Naval Postgraduate School.

Miller, S.D., Combs, C.L., Kidder, S.Q., Lee, T.F., 2012. Assessing moonlight availability for nighttime environmental applications by low-light visible polar-orbiting satellite sensors. J. Atmos. Ocean. Technol. 29, 538–557.

Öhman, Y., 1949. Photoelectric work by the flicker method. In: Stockholms Observatoriums Annaler. 15. pp. 1–8.

Oke, J.B., 1974. Absolute spectral energy distributions for white dwarfs. Astrophys. J. 27, 21–35.

Pedregosa, F., Varoquaux, G., Gramfort, A., Michel, V., Thirion, B., Grisel, O., Blondel, M.,

Prettenhofer, P., Weiss, R., Dubourg, V., Vanderplas, J., Passos, A., Cournapeau, D., Brucher, M., Perrot, M., Duchesnay, E., 2011. Scikit-learn: machine learning in Python. J. Mach. Learn. Res. 12, 2825–2830.

Poynton, C.A., 1998. Rehabilitation of gamma. In: Human Vision and Electronic Imaging III. International Society for Optics and Photonics, pp. 232–250.

Rouse Jr., J., Haas, R., Schell, J., Deering, D., 1974. Monitoring vegetation systems in the Great Plains with ERTS.

Ruhtz, T., Kyba, C.C.M., Posch, T., Puschnig, J., Kuechly, H., 2015. Lichtmesskampagne Zentralraum Oberösterreich. In: Technical Report for Land Oberösterreich prepared by the Freie Universität Berlin.

Sánchez de Miguel, A., 2015. Variacion espacial, temporal y espectral de la contaminacion luminica y sus fuentes: Metodologia y resultados. Ph.D. thesis. Universidad Complutense de Madridhttps://doi.org/10.5281/zenodo.1289932.

Sánchez de Miguel, A., Aubé, M., Zamorano, J., Kocifaj, M., Roby, J., Tapia, C., 2017. Sky quality meter measurements in a colour-changing world. Mon. Not. R. Astron. Soc. 467, 2966–2979.

Sánchez de Miguel, A., García, L., Lindberg Christensen, L., 2015. First use of iss astronaut pictures for light pollution studies. https://www.iau.org/news/pressreleases/detail/iau1510/.

Sánchez de Miguel, A., Gomez Castano, J., Zamorano, J., Pascual, S., Angeles, M., Cayuela, L., Martin Martinez, G., Challupner, P., Kyba, C., 2014. Atlas of astronaut photos of earth at night. Astron. Geophys. 55 36–36.

Schroer, S., Hölker, F., 2016. Impact of Lighting on Flora and Fauna. Springer International Publishing, Cham, pp. 1–33.

Smith, T., Guild, J., 1931. The CIE colorimetric standards and their use. Trans. Opt. Soc. 33, 73.

Stark, H., Brown, S., Wong, K., Stutz, J., Elvidge, C., Pollack, I., Ryerson, T., Dube, W., Wagner, N., Parrish, D., 2011. City lights and urban air. Nat. Geosci. 4, 730–731.

Straizys, V., 1996. The method of synthetic photometry. Balt. Astron. 5, 459–476.

Tapia, C., Sánchez de Miguel, A., Zamorano, J., 2017. LICA-UCM Lamps Spectral Database 2.6.

Tardà, A., Palà, V., Arbiol, R., Pérez, F., Viñas, O., Pipia, L., Martínez, L., 2011. Detección de la iluminación exterior urbana nocturna con el sensor aerotransportado casi 550.

Thapan, K., Arendt, J., Skene, D.J., 2001. An action spectrum for melatonin suppression: evidence for a novel non-rod, non-cone photoreceptor system in humans. J. Physiol. 535, 261–267.

Tucker, C.J., 1979. Red and photographic infrared linear combinations for monitoring vegetation. Remote Sens. Environ. 8, 127–150.

Tucker, C.J., Pinzon, J.E., Brown, M.E., Slayback, D.A., Pak, E.W., Mahoney, R., Vermote, E.F., El Saleous, N., 2005. An extended AVHRR 8-km NDVI dataset compatible with MODIS and spot vegetation NDVI data. Int. J. Remote Sens. 26, 4485–4498.

Walczak, K., Gyuk, G., Kruger, A., Byers, E., Huerta, S., 2017. Nitesat: a high resolution, full-color, light pollution imaging satellite mission. Int. J. Sustainable Light. 19, 48–55.

Wallraff, H.G., 1960. Does celestial navigation exist in animals? In: Cold Spring Harbor Symposia on Quantitative Biology. Cold Spring Harbor Laboratory Press, pp. 451–461. https://doi.org/10.1101/SQB.1960.025.01.047.

Walt, S.v.d., Colbert, S.C., Varoquaux, G., 2011. The numpy array: a structure for efficient numerical computation. Comput. Sci. Eng. 13, 22–30.

Warrant, E., Dacke, M., 2011. Vision and visual navigation in nocturnal insects. Annu. Rev. Entomol. 56, 239–254.

Wikipedia contributors, 2018. Luminous efficacy Wikipedia, the free encyclopedia. http://en.wikipedia.org/w/index.php?title=Luminous_efficacy, Accessed date: 6 June 2018 Online; accessed.

Wyszecki, G., Stiles, W.S., 1982. Color Science. vol. 8 Wiley, New York.

Zheng, Q., Weng, Q., Huang, L., Wang, K., Deng, J., Jiang, R., Ye, Z., Gan, M., 2018. A new source of multi-spectral high spatial resolution night-time light imagery-jl1-3b. Remote Sens. Environ. 215, 300–312.

Zong, Y., 2016. From candle to candela. Nat. Phys. 12, 614.